

Limit regimes of ice formation in turbulent supercooled water

Francesca De Santi¹, Piero Olla^{1*}

¹ *ISAC-CNR and INFN, Sez. Cagliari, I-09042 Monserrato, Italy.*

A study of ice formation in stationary turbulent conditions is carried out in various limit regimes of crystal growth, supercooling and ice entrainment at the water surface. Analytical expressions for the temperature, salinity and ice concentration mean profiles are provided, and the role of fluctuations in ice production is numerically quantified. Lower bounds on the ratio of sensible heat flux to latent heat flux to the atmosphere are derived and their dependence on key parameters such as salt restitution in freezing and ice entrainment in the water column is elucidated.

PACS numbers: 92.10.Rw, 44.35.+c, 47.70.-n

I. INTRODUCTION

Ice production in polar oceans usually occurs in the presence of turbulence and wave motions induced by strong winds. This prevents the formation of a continuous ice layer at the sea surface (thin ice films, called nilas, are indeed observed in very calm conditions). A slurry of ice crystals, with a characteristic milky or greasy appearance, called grease ice, is generated instead. The ice crystals, called frazil crystals or frazil ice, have diameters ranging from 0.01 up to ~ 4 mm and thickness from 1 to 100 μm [1]. If the wind is sufficiently strong, the frazil ice may be blown away, leaving the water surface exposed to the cold air, thus enhancing the ice production and the heat transfer to the atmosphere [3].

Frazil ice is typically present in the Marginal Ice Zone, which is the transition region between the open polar ocean and the continuous ice that covers the central basin, but may also be found under ice shelves and in leads. Ice production is accompanied by salt rejection, and is thus believed to play an important role in stimulating convection in ocean waters. Frazil ice may also contribute to transport of nutrients and other trace elements entrained in its body [4, 5].

Frazil ice formation is a complex phenomenon in which many physical processes play a relevant role [6]. We can list the most important ones.

- Small droplets and foam are continuously lifted up from the water surface and freeze in contact of the cold air. When they return to the water column they act as primary ice seeds.
- If the upper layers of the ocean are sufficiently supercooled, ice crystals grow out of the seeds and reach size up to the millimeter range. New seeds are generated through fragmentation induced by collisions with other crystals (secondary nucleation).
- Part of the crystals are entrained by the turbulence and are transported down the column. Additional

ice production may take place away from the surface if the supercooling is sufficient. Field data indicate that underwater frazil ice and significant supercooling in the water column may indeed be present down to depths of 20–100 m (see e.g. [7]).

Theoretical models for the growth and transport of frazil ice have been developed over the years. In the one-dimensional theory of Omstedt and Svensson [8], the upper ocean was modelled as a turbulent Eckman layer with the sea-ice mixture treated as a continuum. This model was improved in [9] to take into account the size spectrum of the crystals. Ice production under ice shelves was studied in [10], adopting a Boussinesq-like approximation. This latter study was later extended in [11] to account for the size spectrum of the frazil crystals. A detailed study of the precipitation of the frazil crystals on the shelf was carried out in [12]. Large Eddy Simulations (LES) were utilized in [13] to study the frazil ice dynamics under polar ice covers and leads, but no account was taken of the size distribution of the ice crystals. Only recently there has been some attempt to include such information in LES of frazil ice formation in open ocean [14].

Due to the complexity of the process, all these models necessarily rely on parameterization of small scale phenomena and on the introduction of empirical constants. In such circumstances, it may be of some interest to look for limit regimes in which a reduced number of parameters is at play and identification of key physical aspects is simpler. This is precisely the strategy that will be adopted in this paper. The analysis will first focus on the constraints imposed by the conservation laws and the thermodynamics of the process. The case of a homogeneous domain will be examined first. The analysis will then shift to the real problem, i.e. ice production in a water column which is mechanically forced and simultaneously cooled down at the top surface.

II. ICE PRODUCTION: BUDGET EQUATIONS

Let us start by considering ice formation at constant pressure in a thermally isolated, initially supercooled volume of salt water. The water is stirred vigorously

*Email address for correspondence: olla@dsf.unica.it

to maintain uniform conditions and to insure that only small ice crystals are present. The volume is taken small enough for complications associated with differences between temperature and potential temperature, and with the depth dependence of the freezing point, to be negligible. We know that a variation δC in the volume fraction

TABLE I: Physical parameters for salt water at reference temperature $T_B = -2.09^\circ\text{C}$, and total salinity $S_R = 34.5$ psu.

$a_S \simeq 0.0573^\circ\text{C}/\text{psu}$	haline lowering of freezing point.
$a_z \simeq 7.61 \cdot 10^{-4}^\circ\text{C}/\text{m}$	lowering of freezing point with depth.
$\alpha_T \simeq 3.79 \cdot 10^{-4} \text{ m}/(^\circ\text{C s}^2)$	thermal buoyancy coefficient.
$\alpha_S \simeq 7.7 \cdot 10^{-3} \text{ m}/(\text{psu s}^2)$	haline buoyancy coefficient.
$\alpha_C \simeq 1 \text{ m}/\text{s}^2$	ice buoyancy coefficient.
$c_P \simeq 3947 \text{ J}/(\text{kg }^\circ\text{C})$	water specific heat.
$\mathcal{L} \simeq 3.35 \cdot 10^5 \text{ J}/\text{kg}$	specific latent heat of fusion.
$\rho_w \simeq 1030 \text{ kg}/\text{m}^3$	reference water density.
$\rho_i \simeq 920 \text{ kg}/\text{m}^3$	ice density.

of ice leads to a heat release per unit volume in the liquid phase, $\delta Q = \mathcal{L}\rho_i\delta C$, where \mathcal{L} is the latent heat of fusion per unit mass of ice and ρ_i is the ice density. This will produce a temperature increase

$$\delta T = (\hat{\rho}\mathcal{L}/c_P)\delta C \quad (1)$$

in the liquid phase, where we have indicated with

$$\hat{\rho} = \rho_i/\rho_w \simeq 0.89 \quad (2)$$

the density ratio of ice and water and c_P is the water specific heat. We neglect the contribution to the heat flux from the temperature difference between the liquid phase and the ice [12], as it is much smaller than that from the latent heat.

During freezing a fraction $\beta \approx 1$ of the salt that was in the water forming the crystals is expelled to the surroundings [6]. The local salinity can be expressed as the sum of a reference salinity $S_R = 34.5$ psu and a deviation S that is expected in most situations to be small. A volume fraction increase δC in the ice will thus correspond to a decrease $\hat{\rho}\delta C$ of the liquid volume fraction, and to a release of salt per unit volume

$$\delta S = \hat{\rho}\beta S_R\delta C. \quad (3)$$

The water freezing temperature T_i decreases for increasing pressure (depth) and salinity content. For small deviations, we have a linear relation [6]

$$T_i = T_{iR} - a_S S + a_z z, \quad (4)$$

where $-z$ is the depth and $T_{iR} \simeq -2.09^\circ\text{C}$. The decrease of the freezing point from creation of a volume fraction δC of ice will be therefore

$$\delta T_i = -\hat{\rho}a_S\beta S_R\delta C. \quad (5)$$

The resulting supercooling in an initially ice-free water volume at temperature T_0 and salinity anomaly $S_0 = 0$,

after formation of a volume fraction C of ice, will be therefore

$$T - T_i = T_0 - T_{iR} + (a_S\hat{S}_R + \hat{\mathcal{L}})C \quad (6)$$

where

$$\hat{S}_R = \hat{\rho}\beta S_R \quad \text{and} \quad \hat{\mathcal{L}} = \hat{\rho}\mathcal{L}/c_P. \quad (7)$$

From Table I we find $a_S\hat{S}_R \simeq 1.76^\circ\text{C}$ and $\hat{\mathcal{L}} \simeq 75.5^\circ\text{C}$. Warming from latent heat release is more effective in destroying supercooling than freezing point lowering by salinity increase. This implies that ice production can be sustained longer more effectively by cooling down the mass of water than by removing salt.

We can determine the ice volume fraction that can be generated starting from given supercooled condition by equating to zero the final supercooling $T - T_i$. From Eq. (6), we find

$$C_{sat} = \frac{T_{iR} - T_0}{\hat{\mathcal{L}} + a_S\hat{S}_R}. \quad (8)$$

For an initial supercooling $T_0 - T_{iR} = -0.1^\circ\text{C}$, of the order of what is observed in wave-tank experiment [15], and considered as maximum transient supercooling in several models (see e.g. [9, 13, 14]), we would get an ice volume fraction at saturation $C_{sat} \simeq 0.0013$. Is it big or is it small? For a monodisperse suspension of disks of aspect ratio ϵ , the maximum volume fraction compatible with random orientation of the disks is $C \sim \epsilon$. This is what would be obtained if each volume of the fluid of size $\sim R^3$, with R the radius of the disks, contained on the average one disk. Higher volume fractions could be achieved (maintaining random orientation) if smaller crystals filled the gaps among the disks to form a mortar-like assembly. An estimate of the aspect ratio of typical frazil crystals is $\epsilon \approx 1/50$ [11, 12], which would lead to a volume fraction for grease ice $C_g \approx 1/50$. Higher volume fractions would correspond to more compact ice mixtures, with the threshold for solid ice occurring at $C \approx 0.3$ [16]. We note that the above estimate for C_g is an order of magnitude above the saturation concentration C_{sat} predicted by Eq. (8) at an supercooling $T - T_i \approx -0.1^\circ\text{C}$. Transport of heat and salinity away from the production region, together with accumulation of the ice crystals, are therefore necessary for a grease ice layer to be established.

III. TRANSPORT

We follow [8, 12, 13] and others, and coarse grain the dynamics at a scale such that the ice concentration can be treated as a continuum, described by the local volume fraction field $C(\mathbf{r}, t)$. Momentum transport is described by the Navier-Stokes equation, which in the Boussinesq approximation reads

$$(\partial_t + \mathbf{u} \cdot \nabla)\mathbf{u} + (1/\rho_w)\nabla P = \nu\nabla^2\mathbf{u} + (\alpha_T T + \alpha_C C - \alpha_S S)\hat{\mathbf{z}} \quad (9)$$

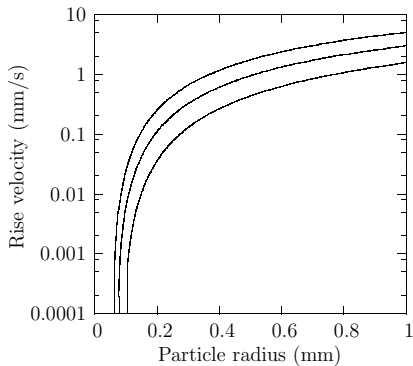


FIG. 1: Rise velocity u_r as a function of the particle radius for different values of the aspect ratio: $\epsilon = 1/100$ (bottom curve); $\epsilon = 1/50$ (middle curve); $\epsilon = 1/30$ (top curve).

(we take the reference system with origin at the water surface, and the vertical z -axis upward directed). The ice buoyancy coefficient can be expressed in term of the ice density ratio as $\alpha_C = g(1 - \rho) \simeq 1 \text{ m}^2/\text{s}$, where $g \simeq 9.8 \text{ m/s}^2$ is the gravitational acceleration. The values of the other coefficients α_T and α_S are listed in Table I. The kinematic viscosity of salt water is $\nu \simeq 1.95 \cdot 10^{-6} \text{ m}^2/\text{s}$.

We can determine the contribution to buoyancy that would be produced by a local increase δC in the ice volume fraction. Using Eqs. (1) and (3) to estimate the local increments of temperature and salinity:

$$\frac{\alpha_T \delta T}{\alpha_C \delta C} \approx 0.06 \quad \text{and} \quad \frac{\alpha_S \delta S}{\alpha_C \delta C} \approx 0.24. \quad (10)$$

This tells us that, while the dominant contribution to ice production saturation comes from latent heat release, the dominant contribution to convection comes directly from ice loading, followed by salinity.

The three fields T , S and C are governed by equations (see e.g. [8])

$$(\partial_t + \mathbf{u} \cdot \nabla)T = \kappa_T \nabla^2 T + \Pi_T, \quad (11)$$

$$(\partial_t + \mathbf{u} \cdot \nabla)S = \kappa_S \nabla^2 S + \Pi_S, \quad (12)$$

$$[\partial_t + (\mathbf{u} + \mathbf{u}_r) \cdot \nabla]C = \Pi_C, \quad (13)$$

where Π_T , Π_S and Π_C are production terms whose form will be specified below. The diffusivity coefficients in Eqs. (11) and (12) are $\kappa_T \simeq 1.4 \cdot 10^{-7} \text{ m}^2/\text{s}$, and $\kappa_S \simeq 7.4 \cdot 10^{-10} \text{ m}^2/\text{s}$, and the molecular diffusivity of the ice crystals is disregarded. Note that we have included in the equation for the ice fraction the rise velocity of the crystals relative to the surrounding water, $\mathbf{u}_r = u_r \hat{\mathbf{z}}$. This is necessarily an average, as crystals of different size and aspect ratio will have different rise velocity. Gosink and Osterkamp [17] provided model equations for u_r , in the case of individual crystals, as a function of their radius and thickness. A plot of such dependence is shown in Fig. 1.

The production terms can be taken in the form, from Eqs. (1) and (3):

$$\Pi_C = \Gamma C; \quad \Pi_S = \hat{S}_R \Gamma C; \quad \Pi_T = \hat{\mathcal{L}} \Gamma C. \quad (14)$$

Usually, a linear dependence of the growth rate Γ on the supercooling is assumed [18],

$$\Gamma = \gamma (T_i - T). \quad (15)$$

The parameter γ depends on the size distribution and the morphology of the crystals, and on the sign of $T_i - T$; it can be interpreted as the inverse time, normalized to the supercooling, required by a crystal to reach mature size. In the case of a mono-disperse distribution, γ can be evaluated following [18, 19]:

$$\gamma \approx \begin{cases} \hat{\gamma}/R^2, & T < T_i, \\ \hat{\gamma}/(\epsilon R^2), & T > T_i, \end{cases} \quad (16)$$

where $\hat{\gamma} \approx 3.7 \cdot 10^{-9} \text{ m}^2/(\text{°C s})^{-1}$. For frazil crystals of radius $R = 1 \text{ mm}$, we would find in supercooled conditions $\gamma \approx 0.0037 (\text{°C s})^{-1}$ and a value larger by a factor ϵ^{-1} in above freezing conditions.

IV. A STATIONARY MODEL

It is likely that a significant portion of grease ice forms during an initial transient in which supercooling is strong [8]. After this, a quasi-stationary regime can be expected, although this is necessarily an idealization, since external conditions (say weather patterns) vary on the same time scale of the process itself. An approximation of statistical stationarity could nevertheless be used to describe the faster processes taking place near the water surface.

We envision a situation in which ice is formed primarily at the water surface. Part of this ice may be blown away by the wind, part of it accumulates at the surface to form a grease ice layer, part of it is entrained in the water column. Additional ice production may thus take place in the water column, provided the supercooling is sufficient.

We assume conditions above freezing and absence of ice at sufficient depth. The depth reached by the frazil ice in the column depends on the ratio between the turbulent velocity and u_r , and on the depth of the supercooled region. A schematic of the processes is presented in Fig. 2. At stationary state, the ice concentration in the water column remains constant and the only variation is assumed to take place at the surface, through changes in the thickness h of the grease ice layer.

Ice formation leads to a downward directed salinity flux in the ice-free region, Φ_S^B , and to a latent heat contribution to the heat flux to the atmosphere Φ_T^L . From Eqs. (1) and (3), we can express the latent heat flux in terms of the salinity flux,

$$\Phi_T^L = -(\hat{\mathcal{L}}/\hat{S}_R)\Phi_S^B. \quad (17)$$

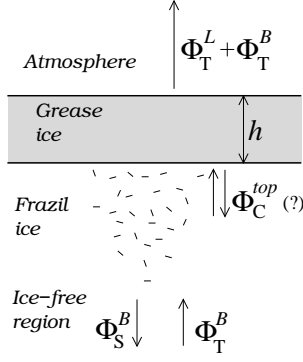


FIG. 2: Sketch of the heat, salinity and ice fluxes generated during build-up of a grease ice layer. The heat flux to the atmosphere is split into latent heat Φ_T^L and sensible heat Φ_T^B contributions. The salinity flux Φ_S^B is downward directed. The question mark indicates that the sign of the frazil ice flux Φ_C^{top} is a priori undetermined.

Putting together with the sensible heat flux Φ_T^B , which coincides with the total heat flux in the ice-free region, we get the total heat flux to the atmosphere

$$\Phi_T^{tot} = \Phi_T^B - (\hat{\mathcal{L}}/\hat{S}_R)\Phi_S^B. \quad (18)$$

It is convenient to introduce supercooling and neutral temperature fields

$$T_o = T - T_{iR} + a_S S \quad (19)$$

and

$$T_n = T - T_{iR} - (\hat{\mathcal{L}}/\hat{S}_R)S. \quad (20)$$

As can be checked from Eqs. (11) and (12), T_o and T_n are decoupled, with only T_o feeling the effect of ice formation and melting. The flux $\Phi_{T_n} = \Phi_T - (\hat{\mathcal{L}}/\hat{S}_R)\Phi_S$ is therefore conserved. We find from Eq. (18),

$$\Phi_{T_n} = \Phi_T^{tot}. \quad (21)$$

The temperature and salinity contributions to buoyancy can be expressed in terms of the fields $T_{o,n}$: $T - (\alpha_S/\alpha_T)S \simeq \text{const.} - 8.05 T_o + 9.05 T_n$. We note that fixed T_n , an supercooled condition at large depth will be less stable than one in which the bottom is above freezing.

If we assume that on the average, supercooling in the ice-free region decreases with depth, $T_o' < 0$, and that the heat and salinity fluxes are arranged in consequence,

$$\Phi_{T_o} \equiv \Phi_T^B + a_S \Phi_S^B > 0, \quad (22)$$

we find that the ratio $\mathcal{B} = \Phi_T^B/\Phi_T^{tot}$ of sensible to total heat flux cannot be zero. The minimum value is

$$\mathcal{B}_{min} = \frac{a_S \hat{S}_R}{\hat{\mathcal{L}} + a_S \hat{S}_R}. \quad (23)$$

From Eq. (7), \mathcal{B}_{min} is an increasing function of the salt release coefficient β and is maximum for $\beta = 1$, $\mathcal{B}_{min} \simeq 0.025$. The maximum value $\mathcal{B} = 1$ describes a situation in which $\Phi_T^L = 0$ and there is exact balance between ice production and melting.

A. Frazil ice fluxes in the water column

Frazil ice in the water column acts as a sink term for the supercooling field T_o . Equations (1) and (3) yields conservation of the flux

$$\Phi_{\mathcal{X}} = \Phi_{T_o} - (\hat{\mathcal{L}} + a_S \hat{S}_R)\Phi_C, \quad (24)$$

which is associated with the field

$$\mathcal{X} = T_o - (\hat{\mathcal{L}} + a_S \hat{S}_R)C. \quad (25)$$

A formula analogous to Eq. (21) can be derived,

$$\Phi_{\mathcal{X}} = \Phi_{T_o}^B. \quad (26)$$

As in the case of T_n , the field \mathcal{X} is not affected by ice production.

The frazil ice flux Φ_C in the water column is the sum of the contributions by deposition and turbulent entrainment,

$$\Phi_C = \bar{C}u_r + \overline{\tilde{u}_z \tilde{C}} \quad (27)$$

(overbar and tilde indicate average and fluctuating components). The flux on the top of the column, Φ_C^{top} , will be positive if deposition $\bar{C}u_r$ dominates, negative otherwise. At stationarity, positive Φ_C^{top} necessarily corresponds to ice production exceeding melting in the water column.

Let us introduce the ratio \mathcal{E} of the frazil flux at the top of the column, taken with minus sign, and the total ice production $\Phi_T^L/\hat{\mathcal{L}}$. In terms of the parameter \mathcal{B} ,

$$\Phi_C^{top} = (\mathcal{E}/\hat{\mathcal{L}})(\mathcal{B} - 1)\Phi_T^{tot}. \quad (28)$$

The ratio \mathcal{E} will be positive or negative depending on whether entrainment or deposition dominates; from positive definiteness of the deposition flux, we must have $\mathcal{E} \leq 1$.

We can refine the bound in Eq. (23) by imposing $\Phi_{T_o}^{top} > 0$. From Eq. (24) and the condition that no ice is present at large depth, we have

$$\Phi_{T_o}^{top} = \Phi_{T_o}^B + (\hat{\mathcal{L}} + a_S \hat{S}_R)\Phi_C^{top} > 0. \quad (29)$$

From definition of T_o and T_n , we have $\Phi_{T_o} = \Phi_T^B + a_S \Phi_S^B$ and $\Phi_{T_n} = \Phi_T^B - (\hat{\mathcal{L}}/\hat{S}_R)\Phi_S^B$. This, together with Eq. (23), allows us to express

$$\Phi_{T_n} = \frac{1 - \mathcal{B}_{min}}{\mathcal{B} - \mathcal{B}_{min}} \Phi_{T_o}^B. \quad (30)$$

Substituting into Eq. (29), we obtain

$$\mathcal{B} > \mathcal{B}_{min}(\mathcal{E}) = \frac{\mathcal{B}_{min} + \mathcal{E}}{1 + \mathcal{E}}. \quad (31)$$

In the limit $\mathcal{B} \rightarrow \mathcal{B}_{min}(\mathcal{E})$, all of the supercooling flux $\Phi_{T_o}^B$ is utilized to melt the frazil ice in the column, and $\Phi_{T_o}^{top} = 0$. For $\mathcal{E} = 0$ (balance of entrainment and deposition), we recover the bound in Eq. (23). The same situation occurs for $\mathcal{E} < 0$ (deposition dominant with respect to entrainment), in which case the bound in Eq. (23) becomes stronger than the one in Eq. (31). In the limit case in which all the ice is entrained in the column, the sensible heat flux must be at least a fraction $\mathcal{B}_{min}(1) \simeq 1/2$ of the total heat flux.

V. THE GREASE ICE LAYER

In order for ice production to be maintained in the grease ice layer—if at all present, it is necessary that the salt released in the process is efficiently transported down the layer and dispersed in the water column. Due to the high viscosity of the medium ($\nu_g \simeq 0.01 \text{ m}^2/\text{s}$), turbulent transport is negligible. A possible transport mechanism of heat and salinity is shear-induced diffusion [20, 21] associated with random fluid motions at the scale of the ice crystals. If the shear is sufficiently strong, temperature and salinity in the grease ice layer will diffuse with identical diffusivity $\kappa_g \gg \kappa_{T,S}$.

We assume uniform properties of the grease ice, $C(\mathbf{r}, t) = C_g$, with γ constant throughout the layer. Equations. (11) and (12) will read in terms of the new variables T_o and T_n , at stationarity,

$$l^2 \partial_z^2 T_o = T_o \quad \text{and} \quad \partial_z^2 T_n = 0, \quad (32)$$

where

$$l \simeq \left(\frac{\kappa_g}{\gamma \hat{C} C_g} \right)^{1/2}. \quad (33)$$

Equation (32) has solution

$$T_o(z) = T_o(0) e^{z/l} + \hat{T}_o (e^{-z/l} - e^{z/l}), \quad (34)$$

$$T_n(z) = T_n(0) + T'_n z. \quad (35)$$

Taking $\gamma \approx 0.003 \text{ (}^\circ\text{C s)}^{-1}$, and $C_g \approx 1/50$, l may range from centimeters ($\kappa_g \approx \kappa_T$), to meters, if one were to identify the effective diffusivity with the effective viscosity of the layer ($\kappa_g \approx 0.01 \text{ m}^2/\text{s}^2$).

Of the two relevant limits $l \ll h$ and $l \gg h$, only the first is of some interest. For $l \gg h$ it is easy to see, by Taylor expansion of Eq. (34), that ice production in the grease ice layer contributes to the heat flux with an $O(h/l)$ correction, so that $\mathcal{B} \simeq 1$ in the absence of ice formation in the water column.

The interest of the opposite limit regime $l \ll h$ lies in the fact that it allows an easier interpretation of the

lower bound in Eq. (23). Let us consider first the case in which ice only forms at $z \simeq 0$.

In this regime, $\hat{T}_o = 0$ in Eq. (34). The second constant T'_n in Eq. (35), is fixed by imposing that there is no salt flux to the atmosphere, $S'(0) = 0$. This gives

$$T'_n = T_o(0)/l. \quad (36)$$

The fact that there is no supercooling at $-l \gg z \gg -h$, $T_o(z) = 0$, implies that temperature and salinity are dominated by T_n and have a linear profile (see Eq. (35)). We can calculate the heat and salinity fluxes $\Phi_T = -\kappa_g T'$ and $\Phi_S = -\kappa_g S'$ in this region. Substituting Eq. (36) and the condition $T_o = 0$ into Eqs. (19) and (20), we get

$$\Phi_T = -\kappa_g \mathcal{B}_{min} T_o(0)/l; \quad (37)$$

$$\Phi_S = (1 - \mathcal{B}_{min}) \kappa_g \hat{S}_R T_o(0)/(\hat{C} l). \quad (38)$$

Since $T_o(-h) = 0$, there will be no melting at the bottom surface and the heat flux right below will still be given by Eq. (37). If the water in that region is ice free, the heat flux will coincide with the sensible heat flux Φ_T^B and exploiting (36) and (21) we obtain $\Phi_T^B = \mathcal{B}_{min} \Phi_T^{tot}$. Thus $\mathcal{B} = \mathcal{B}_{min}$ and the latent heat contribution to the heat flux to the atmosphere is maximum. A situation in which $\mathcal{B} > \mathcal{B}_{min}$ corresponds to ice melting at the bottom of the layer, with the difference $(\mathcal{B} - \mathcal{B}_{min}) \Phi_T^{tot}$ giving precisely the heat required for melting. The same situation would arise if T_o remained close to zero at $z = -h$, but frazil ice were entrained by turbulence and melted down upon reaching the region at $T_o > 0$ at the bottom of the column.

VI. THE WATER COLUMN

Frazil ice production requires strong winds. A minimum wind velocity $u_{wind} = 4.35 \text{ m/s}$ at 10 m above the water surface was suggested in [22] as a necessary condition for frazil ice formation. A turbulent boundary layer forced both by mechanical stress and convection induced by heat and salinity fluxes is thus expected to exist below the grease ice layer.

An estimate of the friction velocity u_* generated under the water surface by the wind stress was provided in [22],

$$u_* \approx A [\hat{\rho}_{air} (1 + u_{wind}/\bar{u})]^{1/2} u_{wind}, \quad (39)$$

where $\hat{\rho}_{air} \approx 10^{-3}$ is the air water density ratio, and a and \bar{u} are empirical constants: $A = 0.028$ and $\bar{u} = 12.3 \text{ m/s}$. A 10-meter wind velocity $u_{wind} = 10 \text{ m/s}$ would lead to a friction velocity

$$u_* \approx 0.01 \text{ m/s}. \quad (40)$$

The strength of the convective forcing can be estimated from the heat flux to the atmosphere. Estimates of the heat flux during frazil ice production events fall in the range

$$\Phi_T^{tot} = 2.5 \cdot 10^{-5} - 10^{-4} \text{ }^\circ\text{C m/s}, \quad (41)$$

corresponding in energy units to $(\rho_w c_P / \mathcal{L}) \Phi_T = 100 - 1000 \text{ W/m}^2$ [8, 14, 22]. From Eqs. (40) and (18) we can define an Obukhov depth signaling transition from a mechanical stress dominated to a thermal convection dominated turbulent region

$$L_T = \frac{u_*^3}{\alpha_T \Phi_T^{tot}} = 30 - 300 \text{ m} \quad (42)$$

(this is clearly a lower bound since the heat flux responsible for convection is only a fraction of Φ_T). The Obukhov depth is going to be reduced by salt release in ice formation. If all the heat ceded to the atmosphere came from ice formation we would get

$$L_S = \frac{\hat{\mathcal{L}} u_*^3}{\alpha_S \hat{S}_R \Phi_T^{tot}} = 3 - 30 \text{ m}, \quad (43)$$

which tells us that already one tenth of Φ_T^{tot} coming from ice formation would be sufficient to invalidate Eq. (42). The estimate in Eq. (43) would be further reduced if ice were transported down the column together with the brine,

$$L_C = \frac{\hat{\mathcal{L}} u_*^3}{\alpha_C \Phi_T^{tot}} = 0.75 - 7.5 \text{ m}. \quad (44)$$

Note, from the second of Eq. (10), that transport down the column of just one quarter of the ice produced at the surface, would be sufficient to counterbalance the destabilizing effect of salinity production. One-dimensional models such as [9, 12] suggest that an ice flux in the water column is indeed present, but is composed mainly of very tiny crystals. This implies large numbers of crystals with a low ice volume fraction. Low values of $-\hat{\mathcal{L}} \Phi_C / \Phi_T^{tot}$ could be inferred from [14] as well. This would suggest that the main contribution to convection is from salt and that the appropriate estimate of the Obukhov depth is that of Eq. (43).

VII. THE TURBULENT BOUNDARY LAYER

Let us focus on the top part of the water column at $z > -L_S$. We assume that a well developed mechanical boundary layer, in which the feedback by C , T_o and T_n on the turbulence can be disregarded, exists. The friction velocity u_* and the Obukhov length L_S provide the natural scales for the velocity fluctuations in that region. A natural scale for the reacting fields C and T_o is the supercooling flux in the ice-free region, $\Phi_{T_o}^B \equiv \Phi_\chi$.

We rescale quantities in terms of L_S , u_* and Φ_χ :

$$\begin{aligned} z &\rightarrow L_S z, \quad t \rightarrow (L_S / u_*) t, \\ T_{o,n} &\rightarrow (\Phi_\chi / u_*) T_{o,n}, \\ C &\rightarrow [u_* (\hat{\mathcal{L}} + a_S \hat{S}_R)]^{-1} \Phi_\chi C. \end{aligned} \quad (45)$$

After rescaling, $\mathcal{X} = T_o - C$. It is convenient to introduce the reacting field

$$\mathcal{Y} = T_o + C. \quad (46)$$

The ice dynamics is simplified considering that only tiny crystals are transported down the column, which have very small rise velocity compared to u_* . This observation is confirmed by numerical simulations [14]. We thus neglect u_r in Eq. (13). Transport in the mechanical boundary layer can be modeled by introducing an eddy diffusivity $\kappa_{turb} \approx -\sigma u_* z$ ($\sigma = 0.4$ is the von Karman constant). Transport equations in dimensionless form for the fields T_n , \mathcal{X} and \mathcal{Y} can then be obtained from Eqs. (11-13):

$$\partial_z(z \partial_z \bar{\mathcal{Y}}) + (1/2)[\overline{\lambda \mathcal{Y}^2} - \overline{\lambda \mathcal{X}^2}] = 0, \quad (47)$$

$$\partial_z(z \partial_z \bar{T}_n) = \partial_z(z \partial_z \bar{\mathcal{X}}) = 0. \quad (48)$$

The parameter

$$\lambda = \frac{H_B u_* \gamma \hat{\mathcal{L}}}{\sigma \alpha_S \hat{S}_R}, \quad (49)$$

with $H_B = (\mathcal{B} - \mathcal{B}_{min}) / (1 - \mathcal{B}_{min})$, gives the relative strength of the contributions to the dynamics from ice formation and transport. It could equivalently be seen as the ratio of the reaction timescale $\Phi_{T_o}^B / (u_* \gamma)$ and the turbulent transport timescale L_S / u_* , which explains the counterintuitive proportionality with u_* . It is important to note that λ , due to the strong dependence of γ on the sign of T_o (see Eq. (16)), is itself a fluctuating quantity.

We can make some estimates. Taking $u_* \approx 0.01 \text{ m/s}$ and assuming above freezing conditions, would give for one-millimeter crystals with $\epsilon = 1/50$, $\lambda \approx H_B$. Smaller crystals lead to larger values of λ , but the effect is counteracted by the fact that such crystals typically have larger ϵ [26]. In realistic situations, we expect λ to be at most $O(1)$.

It is interesting to note that λ vanishes in the limit $\mathcal{B} \rightarrow \mathcal{B}_{min}$, in which case there is no ice in the water column (this corresponds to the limit $\mathcal{E} \rightarrow 0$ in Eq. (31)).

We see from Eq. (48) that the two non-reacting fields T_n and \mathcal{X} obey logarithmic scaling

$$\bar{T}_n(z) = \frac{1}{\sigma} \frac{1 - \mathcal{B}_{min}}{\mathcal{B} - \mathcal{B}_{min}} \ln(-z / \Lambda_n), \quad (50)$$

and

$$\bar{\mathcal{X}}(z) = (1/\sigma) \ln(-z / \Lambda_\chi), \quad (51)$$

where the factors in front the logarithms are $(1/\sigma)$ times the fluxes Φ_{T_n} and Φ_χ expressed in dimensionless form (see Eqs. (24), (30) and (45)).

The two limit regimes $\Lambda_n \ll 1$ and $\Lambda_n \gtrsim 1$, and more important, $\Lambda_\chi \ll 1$ and $\Lambda_\chi \gtrsim 1$, correspond to $\bar{T}_n, \bar{\mathcal{X}} > 0$ and $\bar{T}_n, \bar{\mathcal{X}} < 0$, respectively, in most of the domain. In particular, for $\Lambda_\chi \ll 1$, from positive definiteness of C , most of the domain will be above freezing; for $\Lambda_\chi \gtrsim 1$, either supercooling, or ice, or both will be present.

A. Two limit regimes

For small λ , the dynamics of \mathcal{Y} in the mechanical boundary layer reduces to that of a passive scalar; \mathcal{Y}

and therefore also T_o and C obey in first approximation logarithmic scaling.

For $\lambda \gtrsim 1$, solution of Eq. (47) is complicated by nonlinearity and by the presence of fluctuations. To make analytical progress, we momentarily neglect fluctuations.

We can linearize the dynamics provided $\bar{\mathcal{X}}^2 \simeq \bar{\mathcal{Y}}^2$, meaning that either $\bar{T}_o \simeq \bar{\mathcal{X}}$ and \bar{C} is small, or $\bar{C} \simeq -\bar{\mathcal{X}}$ and \bar{T}_o is small. In the first case $\bar{\mathcal{Y}} \simeq \bar{\mathcal{X}} - \bar{C}$ and Eq. (47) becomes

$$\sigma \partial_z (z \partial_z \bar{C}) + \bar{\lambda} \bar{C} \ln(-z/\Lambda_{\mathcal{X}}) = 0; \quad (52)$$

in the second $\bar{\mathcal{Y}} \simeq -\bar{\mathcal{X}} + \bar{T}_o$ and Eq. (47) becomes

$$\sigma \partial_z (z \partial_z \bar{T}_o) + \bar{\lambda} \bar{T}_o \ln(-z/\Lambda_{\mathcal{X}}) = 0. \quad (53)$$

Equations (52) and (53) are identical in form and describe decay (within logarithms) at depth $-z \sim \bar{\lambda}^{-1}$.

Let us calculate the decay explicitly. We assume that decay takes place in the region of applicability of Eqs. (52) and (53), that is the mechanical boundary layer $z > -1$.

Consider first the case of Eq. (52), in which \bar{C} is small and $\bar{T}_o \simeq \bar{\mathcal{X}}$. In order for such regime to be realized, it is necessary that the entrainment is small on the scale of T_o , i.e. $\Phi_C^{top} \ll 1$. It is also necessary that $T_o > 0$ in the domain of interest, which requires $\Lambda_{\mathcal{X}} \ll \bar{\lambda}^{-1}$. This condition corresponds to studying the melting dynamics of \bar{C} for fixed $\bar{T}_o > 0$.

The singularity at $z \rightarrow \infty$ in Eq. (52) is treated by working in the eikonal representation, $\bar{C} = \exp(W)$ [23]. To leading order in z , Eq. (52) becomes

$$\sigma \lambda z (W')^2 + \ln(-z/\Lambda_{\mathcal{X}}) = 0, \quad (54)$$

which has solution, for $-z \gg \Lambda_{\mathcal{X}}$,

$$W(z) = \pm 2 \sqrt{(-z/(\sigma \lambda)) \ln(-z/\Lambda_{\mathcal{X}})}. \quad (55)$$

We get the asymptotic behavior

$$\bar{C}(z) \sim \exp \left[-2 \sqrt{(-z \bar{\lambda}/\sigma) \ln(-z/\Lambda_{\mathcal{X}})} \right], \quad (56)$$

which leads to the decay depth for $\bar{C}(z)$

$$-z_C \sim |\bar{\lambda} \ln(\bar{\lambda} \Lambda_{\mathcal{X}})|^{-1}. \quad (57)$$

The case in which \bar{T}_o is small and $\bar{C} \simeq -\bar{\mathcal{X}}$ is treated in exactly the same way. We require now $\Phi_C^{top} \simeq 1$, and, in order for \bar{C} to be positive in the domain, $\Lambda_o > 1$ (note that in this case the frazil ice reaches the bottom of the mechanical boundary layer). This corresponds to studying the decay of \bar{T}_o induced by ice formation/melting.

Proceeding with Eq. (53) as in the case of Eq. (52), we obtain for $\bar{T}_o(z)$ the same decay depth as for C , $z_{T_o} = z_C$.

VIII. FLUCTUATIONS

We estimate fluctuations in the mechanical boundary layer by means of a simple Kraichnan model [24, 25], in

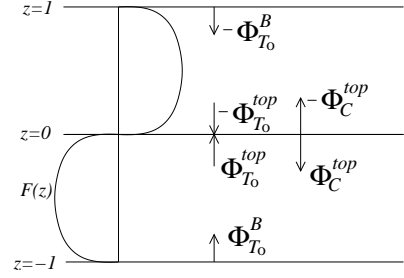


FIG. 3: Sketch of the computation domain.

a periodic 2D domain $[-1, 1] \times [-1, 1]$. We focus on the dynamics of the reacting fields T_o and C . We take x and z as the horizontal and vertical coordinates, with $z = 0$ the water surface and the periodic point $z = \pm 1$ the bottom of the boundary layer ($z = -L_S$ in the original units). The computation domain is thus split in two statistically equivalent mirror sub-domains at $-1 < z < 0$ and $0 < z < 1$. The situation is illustrated in Fig. 3. We continue to work with the dimensionless variables defined in Eq. (45).

A boundary layer structure is imposed on the velocity fluctuations by means of a shape function $F = F(z)$. We write

$$u_x = \bar{u}_x - \partial_z \psi_F, \quad u_z = \partial_x \psi_F, \quad (58)$$

where $\psi_F(\mathbf{r}, t) = F(z)\psi(\mathbf{r}, t)$ and $\psi(\mathbf{r}, t)$ is zero-mean, spatially homogeneous and white in time,

$$\overline{\psi(\mathbf{r}, t) \psi(\mathbf{r}', t')} = \Psi(\mathbf{r} - \mathbf{r}') \delta(t - t'). \quad (59)$$

We take for the shape function

$$F = \prod_{m \in \mathbb{Z}} \tanh[2\pi(z + m)] \quad (60)$$

and for $\bar{u}_x(z)$ a sum of logarithms mimicking the mean velocity profile in a turbulent channel flow.

We have chosen the shape function in such a way that $u_z(0) = 0$ but $u_x(0) \neq 0$, as expected for the turbulent velocity at the free water surface. The fact that $F'(0) \neq 0$, together with periodicity, require however that $F = 0$ and therefore $u_z = 0$ somewhere else in the domain. The choice $F(\pm 1) = 0$ is the one which less affects the dynamics, although it somewhat spoils the interpretation of $z = \pm 1$ as the bottom of the mechanical boundary layer.

We have taken for the spectrum $\Psi_{\mathbf{k}} = \int d^2r e^{-i\mathbf{k} \cdot \mathbf{r}} \Psi(\mathbf{r})$,

$$\Psi_{\mathbf{k}} = A (k^2 + k_0^2)^{-8/3}, \quad (61)$$

which guarantees Richardson scaling for relative diffusion at small separation [25]. The parameter k_0 is a large scale cutoff that we have put equal to 5π . The constant A is

fixed by imposing the condition for the spatial average of the turbulent diffusivity

$$\langle \kappa_{turb} \rangle = \int dt \langle \overline{u_z(\mathbf{r}, t) u_z(\mathbf{r}, 0)} \rangle = 1, \quad (62)$$

which replaces the normalization $u_* = 1$ implicit in Eq. (45).

The presence of input and output fluxes for C and T_o at the boundaries of a periodic domain is mimicked introducing forcing terms at $z = 0$ and $z = -1$ in the transport equations (see Fig. 3). From Eqs. (11-13) and (45), we find (with $z \bmod 2$):

$$(\partial_t + \mathbf{u} \cdot \nabla) T_o = \kappa \nabla^2 T_o - \lambda C T_o + 2[-(\Phi_C^{top} + 1)\delta(z) + \delta(z + 1)], \quad (63)$$

$$[\partial_t + (\mathbf{u} + \mathbf{u}_r) \cdot \nabla] C = \kappa \nabla^2 C - \lambda C T_o - 2\Phi_C^{top}\delta(z), \quad (64)$$

where κ is understood as the turbulent diffusivity of the unresolved eddies below the spatial discretization scale.

Taking the difference of Eqs. (63) and (64), we see that the spatial average of $\mathcal{X} = T_o - C$ is conserved, $(d/dt)\langle \mathcal{X} \rangle = 0$, which is equivalent to the statement on conservation of $\Phi_{\mathcal{X}}$ in the previous section.

We have solved numerically the system of equations (63-64), by means of a pseudospectral code on a 256×256 grid, taking $\kappa = 10^{-3}$. We have smoothed the white noise in Eq. (59) by replacing the Fourier modes $\psi_{\mathbf{k}}(t)$ with an Ornstein-Uhlenbeck processes with correlation time below the diffusion time at the discretization scale. An Adam-Bashford integration scheme has been used for advancement in time [27, 28]. A snapshot of the fields C and T_o is shown Fig. 4.

We have taken as control parameters for the simulations, $\lambda_- \equiv \lambda|_{T_o < 0}$, ϵ , Φ_C^{top} and $\langle \mathcal{X} \rangle$. In particular, we concentrate on the three cases $\lambda_- = 1$, $\lambda_- = 0.1$ and $\lambda_- = 0.02$, which would correspond for $u_* = 1$ m/s to crystal radius $R \approx 0.14$ mm, $R \approx 0.45$ mm and $R \approx 1$ mm. We take $\epsilon = 1/50$ for the largest crystal and $\epsilon = 1/5$ for the smaller ones, in accordance to observations in [26].

We have put $\bar{u}_x(z) = 0$, as inclusion of a non-zero horizontal mean velocity profile has been observed to produce negligible effects on the dynamics. As done in Sec. VII, we put $\mathbf{u}_r = 0$, which is appropriate for the smallest crystals, but may be a rough approximation for the largest ones (see Fig. 1).

We have noted that ice may be present at the bottom of the domain, $z = \pm 1$, and may thus generate spurious ice fluxes. To evaluate the effect on the dynamics, we have compared with the case in which an ice sink Φ_C^B is artificially added at $z = \pm 1$, with $\Phi_{T_o}^B \rightarrow \Phi_{T_o}^B + \Phi_C^B$, to guarantee conservation of $\langle \mathcal{X} \rangle$ (with a slight abuse of notation we are using superscript B for the bottom of the numerical domain although the region is not ice-free). As shown in Fig. 5, the dynamics is modified only in the boundary layer region near $z \pm 1$. We thus expect

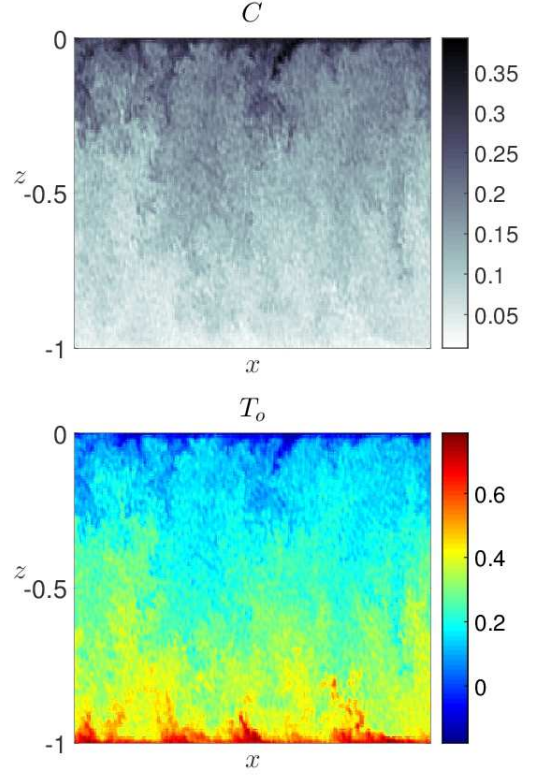


FIG. 4: Snapshot of the ice concentration (top panel) and the supercooling (bottom panel) for $\langle \mathcal{X} \rangle = -\Phi_C^{top} = 0.1$, $\lambda_- = 1$ and $\epsilon = 1/5$.

that the dynamics is properly taken into account by the model for generic values of the parameters.

As a general rule, we find that the fluctuation contribution to the production term $\overline{(\lambda C T_o)_f} = \overline{\lambda C T_o} - \lambda C T_o$ is small, even though the rms component of the individual fields C , T_o and λ are not small at all. We see in Fig. 5, panels *b* and *c*, that ice production fluctuations are concentrated around the transition region from negative to positive T_o . We see in 6 that fluctuations in λ concentrate roughly in the same region, which suggests that a strong contribution to the ice production fluctuations comes from the difference in melting and freezing rates described in Eq. (16).

To determine the effect of the fluctuations of λ on the dynamics, we have compared the case of frazil crystals with $\epsilon = 1$ and $\epsilon = 1/5$. We do not consider the contribution to fluctuations from the dependence of λ on the crystal distribution, which remains undetermined in a description based on the integrated field $C(\mathbf{r}, t)$. We observe in Fig. 7 that for $\epsilon = 1$, $\overline{(\lambda C T_o)_f} = \overline{\lambda C T_o} < 0$, suggesting a picture in which fluctuations of $C T_o$ arise from the cold plumes rich in ice which descends from $z = 0$ into the body of the domain. As shown in Figs. 5c, 7 and 8, for $\epsilon < 1$, fluctuations and mean field components give contribution to ice production of opposite sign in most of the domain.

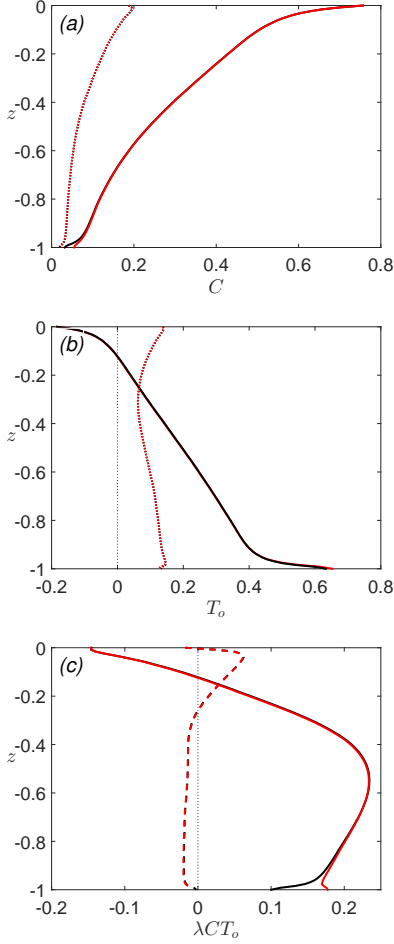


FIG. 5: Effect of an ice sink at $z = \pm 1$ on the vertical profiles of ice concentration (a), supercooling (b) and ice production rate (c); $\Phi_C^B = 0$ in red; $\Phi_C^B = -0.3$ in black; average solid line; rms dotted line. Values of other parameters: $\lambda_- = 1$; $\Phi_C^{top} = -0.5$; $\langle \mathcal{X} \rangle = -0.1$; $\epsilon = 1/5$.

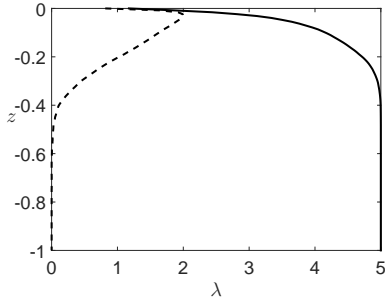


FIG. 6: Vertical profile of λ . Average solid; rms dotted. Values of the parameters $\lambda_- = 1$; $-\Phi_C^{top} = \langle \mathcal{X} \rangle = 0.1$; $\epsilon = 1/5$.

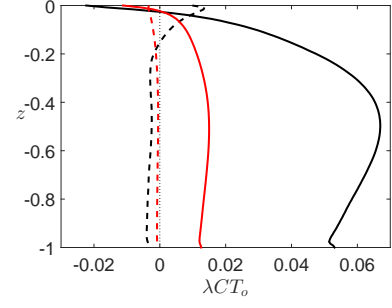


FIG. 7: Vertical profiles of the ice production for different values of ϵ . $\epsilon = 1$ in red, $\epsilon = 1/5$ in black; mean field contribution $\bar{\lambda} \bar{C} \bar{T}_o$ solid line, fluctuation contribution $\overline{(\lambda C T_o)_f}$ dotted line. Values of other parameters: $\lambda_- = -\Phi_C = \langle \mathcal{X} \rangle = 0.1$.

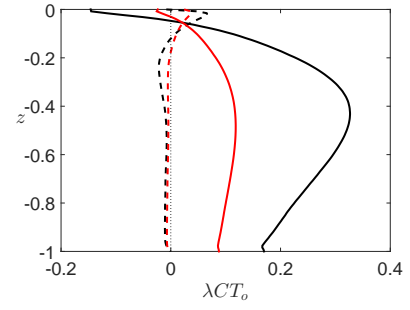


FIG. 8: Same as Fig. 7 for different values of ϵ and λ . $\lambda_- = 0.02$, $\epsilon = 1/50$ in red; $\lambda_- = 1$, $\epsilon = 1/5$ in black.

Fluctuations become negligible deeper in the column, where melting is dominant. This tells us that the mean field analysis in the previous section may be appropriate for the decay of C (see Eq. (57)), but not for that of \bar{T}_o , in which case fluctuations in the sign of T_o are important.

IX. CONCLUSION

We have studied ice formation in a turbulent supercooled water column, in stationary conditions, as a balance of fluxes of heat, salinity and frazil ice.

Our main result is a lower bound on the fraction of sensible heat flux over the total heat flux to the atmosphere. The bound depends solely on the assumption of supercooling decreasing steadily with depth, stationarity and presence of an ice-free region at sufficient depth in the column. The heat flux to the atmosphere cannot be due solely to ice production in stationary conditions; a sensible heat component must always be present, associated with salt release during freezing. The lower bound is an increasing function of the ratio of the rate of entrainment of ice in the column and the total ice production and of the salt restitution in freezing.

Under the same assumptions, we find that the melting process is slower than transport in the mechanical boundary layer at the top of the water column. Thus, in the presence of entrainment, a substantial amount of ice is expected at the bottom of the layer.

Focusing on some limit configurations, we have derived analytical expressions for the vertical profiles of salinity, temperature and ice concentration in the water column, disregarding fluctuations in the ice production terms. The analysis has been carried out under the assumption of small rise velocity of the ice crystals, but it could be generalized to account for such effect.

We have then studied the fluctuation contribution by means of a two-dimensional Kraichnan model for the transport of the salinity, temperature and ice concentration fields.

Our analysis suggests that the fluctuation contribution to ice formation is small for all parameters of interest. It is of course possible that this is a bogus effect from the

particular model utilized. A more appealing explanation is that a stationary condition, allowing mean profiles for the transported quantities to be established, lessens the role of fluctuations. At least limited to stationary condition, the use of simple one-dimensional models may therefore be sufficient to describe the ice dynamics in the water body, the main challenge remaining the proper modelling of processes in the immediate vicinity of the water surface.

Acknowledgements

This research was supported by FP7 EU project ICE-ARC (Grant agreement No. 603887), by MIUR-PNRA, PANACEA project (Grant No. 2013/AN.2.02) and by COST Action grant MP1305.

References

-
- [1] S. Martin, Frazil ice in rivers and oceans. *Ann. Rev. Fluid Mech.* **91** (1981) 756
 - [2] S. Martin, and P. Kauffman, A field and laboratory study of wave damping by grease ice. *J. Glaciol.* **26** (1981) 883
 - [3] A. Alam and J.A. Curry, Evolution of new ice and turbulent fluxes over freezing winter leads. *J. Geophys. Res.* **103C** (1998) 15783
 - [4] H. Eicken, J. Kolatschek, J. Freitag, F. Lindemann, H. Kassen and I. Dimitrenko, A key source area and constraints on entrainment for basin-scale sediment transport by Arctic sea ice. *Geophys. Res. Lett.* **27** (2000) 1919
 - [5] L.H. Smedsrud, Frazil ice entrainment of sediment: large tank laboratory experiments. *J. Glaciol.* **47** (2001) 461
 - [6] S.F. Daly, Evolution of frazil ice in natural water bodies. In: S.F. Daly (Ed.), *International Association for Hydraulic Research Working group on Thermal Regimes: Report on Frazil Ice*, US Army Cold Regions Research and Engineering Laboratory, Hanover, New Hampshire, 1994, p. 11.
 - [7] I.A. Dimitrenko et al. *J. Geophys. Res. Oceans* **115**, C05015 (2010).
 - [8] A. Omstedt and U. Svensson, Modelling supercooling and ice formation in a turbulent Eckman layer. *J. Geophys. Res.* **89C** (1984) 735
 - [9] U. Svensson and A. Omstedt, Simulation of supercooling and size distribution in frazil ice dynamics. *Cold Reg. Sci. Technol.* **22** (1998) 221
 - [10] A. Jenkins and A. Bombosch Modelling the effects of frazil ice crystals on the dynamics and thermodynamics of ice shelf water plumes. *J. Geophys. Res.* **100C** (1995) 6967
 - [11] L.H. Smedsrud and A.D. Jenkins, Frazil ice formation in an ice shelf water plume. *J. Geophys. Res.* **109C** (2004) C03025
 - [12] P.R. Holland and D.L. Feltham Frazil dynamics and precipitation in a water column with depth dependent supercooling. *J. Fluid Mech.* **530** (2005) 101
 - [13] E.D. Skillingstad and D.W. Dembo, Turbulence beneath sea ice and leads: a coupled sea ice/large eddy simulation study. *J. Geophys. Res.* **106C** (2001) 2477
 - [14] Y. Matsumura and K.I. Ohshima, Lagrangian model of frazil ice in the ocean. *Ann. Glaciol.* **56** (2015) 373
 - [15] S. Ushio and M. Wakatsuchi, A laboratory study of supercooling and frazil ice production processes in winter coastal polynias. *J. Geophys. Res.* **98C** (1993) 20321
 - [16] S. Maus and S. De la Rosa, Salinity and solid fraction of frazil and grease ice. *J. Glaciol.* **58** (2012) 594
 - [17] J.P. Gosink and T.E. Osterkamp, Measurements and analyses of velocity profiles and frazil ice-crystals rise velocities during periods of frazil ice formation in rivers. *Ann. Glaciol.* **4** (1983) 79
 - [18] L. Hammar and H.T. Shen, Frazil evolution in channels. *J. Hydraul. Res.* **33** (1995) 291
 - [19] P.R. Holland, D.L. Feltham and S. Daly, On the Nusselt number for frazil ice growth a correction to Frazil evolution in channels by Lars Hammar and Hung-Tao Shen. *J. Hydraul. Res.* **45** (2007) 421
 - [20] L.G. Leal, Macroscopic transport properties of a sheared suspension. *J. Colloid Interface Sci.* **296** (1977) 58
 - [21] B. Metzger, O. Rahli and X. Yin, Heat transfer across sheared suspensions: role of the shear-induced suspension. *J. Fluid Mech.* **724** (2013) 527
 - [22] J. Bauer and S. Martin, A model of grease ice growth in small leads. *J. Geophys. Res.* **88** (1983) 2917
 - [23] C.M. Bender and S.A. Orszag, *Advanced mathematical methods for scientists and engineers*. McGraw-Hill, New York, 1979
 - [24] R. H. Kraichnan, Small-scale structure of a scalar field convected by turbulence. *Phys. Fluids* **11** (1968) 945-963
 - [25] G. Falkovich, K. Gawedzki & M. Vergassola, Particles and fields in fluid turbulence. *Rev. Mod. Phys.* **73** (2001) 913
 - [26] T.R. Ghobrial, M.R. Loewen, & F.E. Hicks Characterizing suspended frazil ice in rivers using upward looking sonars. *Cold Regions Sci. Technol.* **86**, 113 (2013)
 - [27] D. Elhmaidi, A. Provenzale, & A. Babiano, Elementary topology of two-dimensional turbulence from a

- Lagrangian viewpoint and single-particle dispersion. *J. Fluid Mech.* **257** (1993) 533
- [28] D. Elhmaildi, J. von Hardenberg, & A. Provenzale, Dissipation and Filament Instability in Two-Dimensional Turbulence. *Phys. Rev. Lett.* **95** (2005) 014503